NIH Public Access
Author Manuscript
Lab Chip. Author manuscript; available in PMC 2010 September 2.

Published in final edited form as:
Lab Chip. 2009 June 7; 9(11): 1567–1575. doi:10.1039/b819818g.

Fundamentals of magnet-actuated droplet manipulation on an open hydrophobic surface†

Zhicheng Long, **Abhishek M. Shetty**, **Michael J. Solomon**, and **Ronald G. Larson**
Department of Chemical Engineering, University of Michigan, Ann Arbor, MI, 48109, USA

Abstract

We systematically investigate droplet movement, coalescence, and splitting on an open hydrophobic surface. These processes are actuated by magnetic beads internalized in an oil-coated aqueous droplet using an external magnet. Results are organized into an 'operating diagram' that describes regions of droplet stable motion, breakage, and release from the magnet. The results are explained theoretically with a simple model that balances magnetic, friction, and capillary-induced drag forces and includes the effects of particle type, droplet size, surrounding oil layer, surface tension, and viscosity. Finally, we discuss the implications of the results for the design of magnet-actuated droplet systems for applications such as nucleic acid purification, immunoassay and drug delivery.

1. Introduction

Automatic microfluidic manipulation is one of the most critical tasks that must be performed by lab-on-a-chip devices, which aim to integrate various chemical or biological functions on small microchips. Early-generation microfluidic systems, typically using single-phase fluids in microchannels, have realized significant progress towards the development of practical devices for miniaturized biochemical assays.[1–5] However, these continuous-fluid systems often need complicated micropumps and microvalves, or even bulky peripheral apparatus, to drive or direct the liquid through the channel networks, impeding miniaturization and ease of commercialization. Recently, microdroplet-based microfluidic systems have attracted considerable attention.[6,7] Compared to the continuous-flow systems, the manipulation of discrete microdrops can offer higher flexibility, less sample consumption, and lower costs for device fabrication, especially when the droplets are manipulated on an open surface.

Several methods have been used to actuate small droplets on a planar surface, including electrowetting,[8,9] dielectrophoresis,[10] and magnetism.[11–13] Although "digital microfluidics" mostly based on electrowetting has attracted considerable attention, the use of magnetic particles to manipulate a droplet in which particles are suspended has some special advantages. The variety of magnetic particles that are available, including ones capable of adsorbing nucleic acids or other biomolecules, offers a functional support for biomolecular separation and reaction. Also, magnetic particles and droplets are very easy to manipulate and thus can reduce the cost and the size of the controlling apparatus. Magnetic particles have been used to transport small volumes of liquids on miniaturized devices. For example, Garcia *et al*.[14,15] studied the motion of viscous drops on a super-hydrophobic surface due to magnetic gradients. Ohashi *et al*.[16] developed a droplet-based PCR device based on magnetic transport. Nguyen *et al*.[17,18]

†Electronic supplementary information (ESI) available: Droplet merging in a thin (video S1) or thick (video S2) oil shell. See DOI: 10.1039/b819818g

Copyright © The Royal Society of Chemistry 2009

rlarson@umich.edu; Fax: +1 734 763 0459.

NIH-PA Author Manuscript
NIH-PA Author Manuscript
NIH-PA Author Manuscript

NIH-PA Author Manuscript

NIH-PA Author Manuscript

NIH-PA Author Manuscript

reported experimental results on kinematics and deformation of ferrofluid droplets driven by planar magnetic coils. They also designed a novel circular closed-loop ferrofluid-driven microchip for rapid PCR.[19,20] Magnetic-bead based bio-seperations and bioreactions have also been implemented on planar microfluidic platforms. Shikida *et al*.[21–23] reported a magnetic bead-cluster handling system that splits droplets by driving them from one well to the next through a narrow interconnect. Lehmann *et al*.[11,24,25] demonstrated a flexible method that uses magnetic beads for extraction/fusion in a mini oil tank with a hydrophobic bottom. Rather than using an external magnet, they fabricated an array of coils on a PCB plate to generate a gradient in magnetic field.

Pipper and co-workers[12] presented a fully integrated microdroplet system for virus detection, in which all procedures, including cell lysis, RNA extraction and purification, and real time RT-PCR, were performed by manipulating the magnetic beads within arrayed micro-drops. More recently, the same group has extended this technique to the purification of specific cell types and to the amplification of DNA extracted from these cells.[13] In their system, the droplet-encased magnetic beads are not only a solid support for biomolecular adsorption, but also a carrier for droplet transport. One might imagine many additional applications for such an approach, in which all of the fundamental fluidic operations, such as droplet transport, mixing, and magnetic particle extraction, are flexibly assembled on a simple platform. Despite this potential, the full capability of magnetic actuation for droplet manipulation has not been exploited. In general, the range of attainable conditions, such as droplet volumes, masses of particles that can be contained in the droplets, speeds of droplet motion, conditions for droplet breakage or merger, *etc*., are not known.

In this paper, we explore the range of conditions under which magnetic force actuation can be used for microdroplet manipulation on an open surface. For the first time, we present an "operating diagram" to illustrate the conditions under which one might easily switch between bead extraction and droplet transport. We also study the effects of particle type, droplet size, surface tension, viscosity and effect of oil coating on droplet kinematics. We develop a simple force-balance model to explain our experimental observations. Finally we also present design suggestions for practical magnet-actuated droplet systems.

2. Experimental

2.1 Droplet actuation platform

The testing platform used in our study is illustrated in Fig. 1. Aqueous droplets sealed by a thin layer of silicone oil (S159–500, Fisher Scientific Inc.) are placed on a Teflon-coated glass slide. Hydrophilic magnetic particles are suspended in the aqueous phase. An external Nd–Fe–B magnet (BX044, K&J Magnetics Inc., with a surface field of 4480 Gauss) is placed 0.6 mm beneath the slide holder and is used for droplet manipulation. The magnet is mounted on a linear translation stage (T-LLS105, Zaber Technologies Inc., Canada) so that its displacement can be precisely controlled.

Teflon AF 1600 (1% solution in FC-75 Fluorinert, from DuPont) was used to generate a smooth hydrophobic surface on glass slides. To enhance the adhesion between the Teflon film and the glass substrate, the piranha-cleaned glass slides were first immersed in 1% 1H,1H,2H,2H-perfluorodecyltriethoxysilane solution (in isopropanol, with 5% water and a drop of 0.1N HCl) for 30 s. They were then rinsed with isopropanol and dried at 110 °C for 15 min. A thin solution layer of Teflon was then spin-coated onto the fluorosilane-treated slides and sequentially baked at 110 °C for 10 min, 165 °C for 5 min and 330 °C for 15 min. The resulting Teflon film had a thickness of 100–300 nm.

NIH-PA Author Manuscript

NIH-PA Author Manuscript

NIH-PA Author Manuscript

2.2 Droplet manipulations

The oil-coated and bead-containing droplets were introduced onto the hydrophobic surface by precision pipetting. In our experiments, the desired amount of surrounding oil layer, aqueous phase (typically DI water) and the suspension of magnetic beads were sequentially added and which spontaneously formed the droplets. Fig. 1 illustrates the behaviors of droplets and droplet-encased beads in magnet-driven droplet manipulations. First, the suspended magnetic particles within the aqueous droplet are attracted to the bottom of the droplet by the magnetic force. When the magnet is moved horizontally, the particles follow the magnet until they reach the contact line, where they form a compact cluster at the leading edge of the aqueous droplet. Second, the magnetic pulling force acting on the bead-cluster is transferred to the water/oil interface and deforms the droplet. Thereafter, two distinct operations can be achieved. One is droplet movement, achieved when the magnet-driven motion of the magnetic particles pulls the entire oil-ringed droplet. The other is bead-cluster extraction, achieved when a small particle-containing droplet is split out of the mother droplet. Here, we investigate these two processes under various operating conditions and generate an “operating diagram” in the form of a plot of droplet velocity *vs*. magnetic bead loading. In addition, we observe droplet movement, splitting and merging and record these events using a CCD-camera mounted on a stereo microscope (Zeiss Stemi 2000C).

3. Results and discussion

3.1 Droplet kinematics and operating diagram

As shown in Fig. 1, droplet transport and particle extraction are the two most important operations in magnetism-based droplet manipulation systems. In previous bio-separations and bio-reactions involving magnetic-bead-containing droplets, the encased magnetic particles were separately used either as a droplet driver[14,16] or as an extractable solid support.[11,12,21,26] However, in most of these cases droplet motion and bead extraction were not easily integrated operations. So it often proved to be necessary to take measures to diminish the interference between droplet motion and bead separation. For example, to facilitate the bead extraction from the mother droplet, Shikida *et al*.[21–23] used a narrow channel/gate to block the droplet and keep it from being dragged along by the magnet motion while the magnetic force pulled a smaller bead-containing droplet from it. Alternatively, Lehmann *et al.*[11,24,25] created hydrophilic/hydrophobic patterns to immobilize the aqueous droplets on the bottom surface. Super-hydrophobic surfaces and small droplets size are often adopted for droplet transport. Creating these special surfaces or special topographies to manipulate droplets adds to the difficulties of device fabrication. An exception is the latest work of Pipper *et al*., who combined solid phase extraction (droplet splitting) with clockwork PCR, using droplet transport to cycle the droplet to zones imposing the different temperatures needed for PCR.[13] In their experiments, which rotated the magnet at a fixed high speed, only droplets smaller than 10 μL could be transported stably without splitting.

From the above, we recognize that ease of switching between droplet motion and particle extraction is the key to flexible operations in magnetism-based droplet systems. We therefore investigate here the droplet operations that occur at various magnet velocities and magnetic particle loadings. We organize our results into an ‘operating diagram’, shown in Fig. 2 for the case of a 50 μL droplet. It has three distinct operating regions: steady droplet transport, particle extraction, and magnet disengagement. Droplet transport occurs at low magnet speeds, while particle extraction requires a higher speed and a higher loading. Magnet disengagement occurs at high velocities where the magnet leads the droplet by a distance too great for the magnetic field to pull the droplet. Fig. 2b shows images corresponding to the different operating conditions marked in Fig. 2a. These images show that droplets follow the magnetic bead cluster until the cluster outruns the droplet, breaking off a new, smaller droplet. A higher magnet speed

NIH-PA Author Manuscript

NIH-PA Author Manuscript

NIH-PA Author Manuscript

results in a shorter run-up distance before splitting occurs. The operating diagram indicates that one can flexibly switch between droplet motion and particle extraction simply by varying the magnet velocity. Furthermore, it shows how one can easily implement and assemble all necessary operations, whether droplet transport or bead cluster handling, onto a simple open hydrophobic surface without complicated microfabrication.

3.2 Force balance model

We now develop a simple force-balance model to explain the operating diagram. In the present platform, the droplet kinematics and operation outcomes are determined by the subtle balances between the magnetic force (F_m) acting on the bead-clusters, the capillary force (F_c) induced by the droplet deformation and the frictional force (F_f) between the oil-coated droplet and the substrate surface. Note that we here only list the horizontal components of the three forces.

Magnetic force, F_m—

$$F_m = \left(\frac{M}{\rho}\right)\chi\frac{B_m}{\mu_0}\nabla B_m \tag{1}$$

Here M is the mass of the magnetic bead cluster, ρ is the mass density of the magnetic bead material, χ is the magnetic susceptibility of the beads, B_m is the magnetic field applied and μ_0 is the permittivity of free space.[27] From eqn (1) we can obtain a maximum magnetic force that can be applied to the droplet along the magnet motion axis:

$$F_{m,\max} = K_{m,\max}\chi\left(\frac{M}{\rho}\right) \tag{2}$$

where $K_{m,max}$ is the maximum value of $\frac{B_m}{\mu_0}\nabla B_m$ that can be attained for the given magnet and device geometry.

Frictional force, F_f—

$$F_f \cong K_f R_b \mu_{oil} U \tag{3}$$

Here K_f is the friction constant, R_b is the radius of the bottom contact area between the oil-ringed droplet and the substrate, μ is the viscosity of the oil and U is the velocity of the drop.[18,28] Note that the dynamic friction is proportional to the base radius of the oil-coated droplet, not its contact area with the substrate, because it has been found that viscous drag in the vicinity of the contact line dominates the sliding friction for small drops, whose radius is of the order of the capillary length, $k^{-1} = \left(\frac{\gamma_{oil}}{\rho g}\right)^{\frac{1}{2}}$, or smaller.[28] Here γ_{oil} is the surface tension of the surrounding oil phase, ρ is the fluid density, and g is the acceleration due to gravity.

Capillary force, F_c—When a magnet is moved away from a droplet, magnetic particles within the droplet press against the side of the droplet, producing droplet deformation. This deformation creates a capillary force, which holds the particles within the droplet. Beyond a maximum sustainable capillary force, the particle clump will break off a smaller droplet containing the particles. The capillary force at which this occurs has been given by[22]

NIH-PA Author Manuscript

NIH-PA Author Manuscript

NIH-PA Author Manuscript

$$F_{c,\max}=6^{\frac{1}{3}}\pi^{\frac{2}{3}}\gamma_{o-w}\left(\frac{M}{\rho}\right)^{\frac{1}{2}} \tag{4}$$

This maximum capillary force is proportional to the radius of the compact bead-cluster, which is proportional to the cube root of the particle volume M/ρ, assuming that the break-away droplet is just big enough to contain the particle clump which is assumed to be in a close-packed spherical structure. It is also proportional to the interfacial tension $\gamma_{o\text{-}w}$ between the oil layer and water. Note that this crude approximation neglects the complex shape the droplet takes on just prior to breakup, and any influence on that shape produced by the substrate. Thus, despite the inclusion of geometric pre-factors in eqn (4), the equation is really no better than a scaling formula, whose pre-factor could differ considerably from the given one. We also note that if the substrate wettability (solid surface tension) were to play a role, then eqn (4) would not even be a valid scaling law. However, since our substrate is completely wet by the fluid encapsulating the droplet, we do not believe that the wettability of the substrate needs to be considered in our experiments. Finally, the above equation assumes that the dominant fluid–fluid interfacial tension is that of the oil–water interface, which is higher than that of the oil–air interface, and must deform more as well.

The force analysis of the three distinct regions in the operating diagram is shown in Fig. 3.

Region 1. In this region steady transport of the droplet takes place. Here the magnetic force, F_m, is exactly balanced by the frictional force, F_f, ensuring that the droplet and the magnet move at the same speed.

Region 2. Magnet detachment occurs in this region. Both the frictional force, F_f, and the maximum capillary force are greater than $F_{m,\,max}$.

Region 3. In this region, $F_{m,\,max}$ is greater than $F_{c,\,max}$ but $F_{c,\,max}$ is smaller than friction force; this means that the magnetic pulling force acting on the bead cluster overcomes the interfacial force and a small bead droplet will be split off.

In the operating diagram, along the operating boundary OB1, we have

$$F_{\mathrm{m,max}}=F_{\mathrm{f}} \tag{5}$$

Thus, substituting from eqn (2) and (4), we get

$$K_{m,\max}\chi\left(\frac{M}{\rho}\right)=K_f R_b \mu_{oil} U_{pulloff} \tag{6}$$

Rearranging gives

$$U_{pulloff}=\frac{K_{m,\max}\chi\left(\frac{M}{\rho}\right)}{K_f R_b \mu_{oil}} \tag{7}$$

The velocity of the droplet along line OB1 varies linearly with magnetic loading of the droplet and is inversely proportional to the viscosity of the drop and the contact radius of the droplet

NIH-PA Author Manuscript

NIH-PA Author Manuscript

NIH-PA Author Manuscript

with the substrate. This is the "pull-off" velocity since above this velocity the magnetic force is too weak to tow the droplet behind the moving magnet.

Along the boundary OB2,

$$F_{c,max}=F_f \tag{8}$$

Substituting from eqn (3) and (4) gives

$$6^{\frac{1}{3}}\pi^{\frac{2}{3}}\gamma_{o-w}\left(\frac{M}{\rho}\right)^{\frac{1}{3}}=K_f R_b \mu_{oil} U_{breakup} \tag{9}$$

which rearranges into

$$U_{breakup}=\frac{6^{\frac{1}{3}}\pi^{\frac{2}{3}}\gamma_{o-w}\left(\frac{M}{\rho}\right)^{\frac{1}{3}}}{K_f R_b \mu_{oil}} \tag{10}$$

The velocity of the droplet along OB2 follows a power law relationship with magnetic loading, $U \sim M^{1/3}$ and is inversely proportional to the viscosity of the drop and to the contact radius of the droplet. This is the "breakup" velocity since above this velocity the magnetic particles can be separated from the original droplet.

Boundary OB3 stands for the minimum particle loading (M_{min}) required for producing a strong enough magnetic force to overcome the interfacial tension, and allow droplet breakup to occur. If we ignore the fact that viscous forces inside the moving droplet may prevent all the particles from aggregating at the front edge (see later discussion), OB3 should be a vertical line on the operating diagram. Practically, M_{min} can be estimated from the operating diagram where the operating boundaries OB1 and OB2 intersect. At this point,

$$F_{c,max}=F_{m,max} \tag{11}$$

or,

$$6^{\frac{1}{3}}\pi^{\frac{2}{3}}\gamma_{o-w}\left(\frac{M_{min}}{\rho}\right)^{\frac{1}{3}}=K_{m,max}\chi\left(\frac{M_{min}}{\rho}\right) \tag{12}$$

which is rearranged to

$$M_{min}=\frac{\pi\rho 6^{\frac{1}{2}}\gamma_{o-w}^{\frac{3}{2}}}{(\chi K_{m,max})^{\frac{3}{2}}} \tag{13}$$

It is evident from the above equation that the minimum particle loading required for splitting depends on the kind of magnetic particles used, the interfacial tension, and characteristics of the applied magnetic field.

NIH-PA Author Manuscript

NIH-PA Author Manuscript

NIH-PA Author Manuscript

When fixing other parameters and only varying the droplet size, eqn (7) and (10) can be further simplified as

$$U_{OB1} = \frac{\alpha}{R_b} M \tag{14}$$

$$U_{OB2} = \frac{\beta}{R_b} M^{\frac{1}{3}} \tag{15}$$

Here α and β are two constants and are given by the following expressions.

$$\alpha = \frac{K_{m,\max} \chi}{K_f \mu_{oil} \rho} \tag{16}$$

$$\beta = \frac{6^{\frac{1}{3}} \pi^{\frac{2}{3}} \gamma_{o-w}}{K_f \mu_{oil} \rho^{\frac{1}{3}}} \tag{17}$$

The values of α and β can be estimated from previous experimental studies. Due to the relatively small droplet sizes used in our study the friction constant K_f can be estimated from viscous dissipation along the contact line using a Stokes flow approximation. Therefore the friction constant can be written as[28] $K_f = \frac{2\pi c(\theta)}{\gamma} \ln\left(\frac{\Lambda}{\lambda}\right)$, where *c(θ)* is a function of contact angle determined numerically by Kim *et al*. by solving for the flow near a moving contact line, Λ is a length scale up to which the Stokes flow approximation holds, λ is a cut-off molecular length scale which depends on the liquid molecules and the surface roughness, and γ is a prefactor which Kim *et al*. found experimentally to be around 10^{-2} for the frictional force of droplets sliding down inclined planes. Now Λ is proportional to R_b; the contact angle (θ) of silicone oil on our Teflon-coated surface is around 50°, and the value of *c(θ)* is ~0.8. Using a reasonable value of λ = 10 nm from the literature (the results are very insensitive to λ since it appears in a logarithm), we can estimate the friction constant K_f as ~3400. In our system, the surface tension $\gamma_{o\text{-}w}$ is 0.051 N/m and the viscosity of silicone oil is 0.046 Pa s, so from eqn (17) we get the estimated value of β, to be ~1.0×10^{-3} m^2 s^{-1} $kg^{-1/3}$.

Similarly α can be computed from eqn (16). Since we use a permanent magnet in close proximity to the droplet, the constant $K_{m,\max} = \frac{B_m}{\mu_0} \nabla B_m$ can be computed by approximating the field gradient as $\nabla B_m \approx \frac{B_m}{w}$, where w is the geometrical dimension of the magnet (w = 4 mm in our case) and B_m is estimated as the surface strength of our magnet (0.448 Tesla). So $K_{m,max}$ is estimated to be 4.0×10^7 N m^{-3}. The initial susceptibility of the magnetic beads, χ, is about 0.003 (manufacturer data). Using the above values in eqn (16) gives the α value of ~300 m^2 s^{-1} kg^{-1}. The average values of α and β obtained from our experimental data are 320 m^2 s^{-1} kg^{-1} and 2.7×10^{-3} m^2 s^{-1} $kg^{-1/3}$ respectively, which are both within a factor of three of the calculations from our theory. Fig. 4 plots that experimentally observed OB1 and OB2 for droplets of different sizes along with fits to these data by our model, yielding the fitted values of α and β given above. Note that the prediction is very sensitive to the base radii (R_b)

NIH-PA Author Manuscript

NIH-PA Author Manuscript

NIH-PA Author Manuscript

of the composite droplet. We computed the Bond number (Bo), $Bo=\frac{\rho U^2 R_o}{\gamma_{o-w}}$ to check the effect of gravitational forces on droplet shape. For the range of velocities (1–9 mm/s) employed in our study the values of Bo > 1 were found for droplets larger than 20 μL, which implies that gravitational flattening is not negligible. So we here use experimentally measured base radius for calculation.

The fits to the data are quite good, with the largest deviations occurring at high droplet speeds. In this regard, it should be noted that fragmentation of the surrounding oil layer occurs in our system when the droplet velocity is higher than ~3 mm s^{-1} (see later discussion). This partial oil loss is expected to change the friction radius of the droplet and hence should affect our predictions. As a result, when using the original base radius for calculation, the model fits the experimental data well for large droplets (50 μL, 100 μL and 200 μL) in which splitting occurs at a low velocity, before oil layer fragmentation occurs. However, the model gives predictions of OB2 that lie below the experimental data for small droplets of size 10 μL and 20 μL. Therefore, in Fig. 4, predictions based on the base droplet radius assuming complete oil loss are also provided to account for the effect of oil layer fragmentation on droplet kinematics. These corrected predictions capture the 20 μL data well but still give too low a prediction for OB2 for 10 μL droplets. The reason for this discrepancy might be that the small oil-fragmented droplets are not simply sliding on the surface at high speed as assumed by the model, but that "slipping" and "rolling" are also occurring, as discussed by Hodges *et al*.[29] Nevertheless, at least for larger droplets our model does provide a useful, and simple, guide for estimation of conditions required for droplet transport and particle extraction.

3.3 Important parameters

3.3.1 Magnetic properties—As shown in eqn (1), the magnetic force needed for droplet motion or breakup is determined by the strength and gradient of the magnetic field, as well as by the loading and magnetic susceptibility of the particles. Although other methods such as arrayed coils[11,18,25] could be used to generate a field gradient, these do not eliminate the need for a permanent magnet to provide a strong homogeneous magnetic field, and involve a more complicated fabrication process. So in our system we simply placed a small Nd–Fe–B magnet on a motorized translation stage with the magnet positioned vertically close to the testing plate. This scheme generated strong magnetic fields and allowed easy control of the magnet's motion.

Because of their many applications in bioseparation and bio-reaction, hundreds of different grades and sources of magnetic particles are commercially available. These particles are of either superparamagnetic or ferromagnetic type. Superparamagnetic particles have much broader applications than do ferromagnetic ones in biosciences, due to their easy re-suspension, large surface area and slow sedimentation in sample solutions. Advantages of ferromagnetic particles are their very strong magnetic properties and hence easy manipulation even in viscous media. We compared the droplet movement produced by super-paramagnetic SiMAG particles with that produced by ferro-magnetic SiMAG/MP particles (from Chemicell, Germany) both of which have the same size, density and core material. We found that the ferromagnetic SiMAG/MP particles allow splitting at significantly lower particle loadings than do the super-paramagnetic SiMAG. A mass of only 4 μg of SiMAG/MP particles is large enough to produce break up of a 50 μL droplet while a minimum loading of as high as 32 μg is required to induce breakup with superparamagnetic SiMAG particles. In addition, we also observed that extraction of ferromagnetic particles was more complete than that of the superparamagnetic particles, which means that ferromagnetic particles are more suitable for splitting-dominant applications like DNA/RNA purification. When used as a droplet driver, the ferromagnetic particles can also achieve a higher droplet speed at low loading conditions. However, at a given high loading, these particles did not demonstrate a significantly higher droplet speed than is

NIH-PA Author Manuscript

NIH-PA Author Manuscript

NIH-PA Author Manuscript

obtained from superparamagnetic particles. This is because the maximum speed of the droplet, which corresponds to OB2 on the operating diagram, is determined by the maximum capillary force that can be attained without droplet splitting, rather than the maximum magnetic force.

3.3.2 Droplet size—According to our simple model, the frictional force increases with droplet size and velocity, but both the maximum magnetic force and maximum capillary force are independent of the droplet size and depend only on magnetic particle loading. Consequently, the operating boundaries OB1 and OB2, which represent the maximum velocities that a given droplet can be attained, should shift downward as the droplet size increases (see eqn (7) and (10)). This shift is what is observed in our experimental data (see Fig. 4). This result shows that a large droplet cannot be transported at a high speed, even if the magnetic loading is increased considerably. This is also because the maximum speed of the droplet at high particle loadings is not determined by maximum magnetic force but by the maximum capillary force, which only increases with the cube root of the magnetic particle loading. Undoubtedly, a higher speed could be attained by increasing the interfacial tension between aqueous droplet and the surrounding media. These results demonstrate that magnetism-based droplet manipulation systems are able to transport droplets of up to hundreds of microliters, while 'digital microfluidics', which uses electrowetting phenomena to transport droplets, generally deals with droplets smaller than a few microliters.[8,9]

A large droplet size facilitates splitting, which occurs above line OB2 of the operating diagram, while extracting particles from a very small droplet is challenging. In our experiments, superparamagnetic particles within aqueous droplets smaller than 5 μL were never successfully separated on smooth Teflon®AF surfaces. One solution is to increase the friction coefficient between the droplet and the surface (see further eqn (3) and (8) for justification). We did achieve consistent splitting of 1 μL droplets on a commercially available polytetrafluoroethylene (PTFE) plate, which has a rougher surface than spin-coated Teflon®AF surface. These considerations are important in the design of devices for bioassays, where the size of the droplets determines the amount of material that can be processed in a single droplet, as well as the quantities of reagents that must be used.

3.3.3 Surrounding oil layer—To date, droplet manipulations have always been carried out in the presence of an oil medium. The oil facilitates the droplet manipulation in several ways. Firstly, it lowers the interfacial tension between the aqueous droplet and the surrounding medium, making splitting easier. Oil also prevents droplet evaporation and minimizes contamination. In previous studies the magnetic-bead-containing droplets were usually suspended or immersed in a container of oil,[11,16,24,26] which not only complicates fabrication work but also causes operation issues and imaging problems. Alternatively, in our study, the aqueous droplets were sealed by a thin layer of silicone oil, like the configurations reported by Pipper's group.[12,13] Fig. 5a shows side-view images of the compound droplet (water with oil coating) at various oil loadings and droplet speeds. Since the Teflon surface is both hydrophobic (water repelling) and oleophilic (oil loving), a ring of oil is always observed around the bottom of the aqueous droplet. During transport, the moving aqueous droplet drags the oil ring along. But most of the oil lags behind the droplet due to its higher viscosity, even more so at higher droplet speeds. Some of this trailing oil in some cases even breaks off. The oil loss then reduces the viscous drag force between the oil-ringed droplet and the surface. As a result, a higher maximum velocity for the droplet could be attained and splitting would not occur at the predicted speed. In our system, such fragmentation of the oil layer was found to occur once the droplet speed exceeded ~3 mm/s.

Fig. 5b shows the effect of oil loading on the operating diagram of a 50 μl droplet. The boundaries OB1 and OB2 shift downward as the oil loading increases, which may be attributed to the increasing contact area and the size of the emulsion droplet (see eqn (7) and (10)). In

NIH-PA Author Manuscript

NIH-PA Author Manuscript

NIH-PA Author Manuscript

addition, with increased oil loading, a notable decrease in the minimum loading (M_{min}) required for droplet splitting and particle extraction was also observed. It is also noteworthy that the 'no-oil' case in Fig. 5b is distinctly different from all cases in which oil was used. The plot shows that when oil is absent a higher magnetic loading is required to overcome the static friction of the droplet and achieve droplet motion. The absence of boundary OB2 indicates that a very high magnetic loading or droplet velocity is required to overcome the high interfacial tension to achieve splitting in the absence of an oil coating. However, the higher interfacial tension allows attainment of a faster droplet transport speed without breakup.

3.3.4 Surface tension and viscosity of the aqueous phase—Eqn (7), (10) and (13) show that the interfacial tension of the droplet has a large effect on the operating diagram. The interfacial tension of the droplet in our case depends on the surface tensions of the aqueous and oil phases. We examined several buffer solutions commonly used in DNA purification, including lysis buffer (0.02M SDS), binding buffer (6M GuSCN), wash buffer (70% isopropanol) and elution water.[30] We kept the oil phase constant (0.2 μl silicone oil) and changed the aqueous phase so that we could study the effect of surface tension of the aqueous phase on the operating diagram. The effects of surface tension on operating boundaries OB1 and OB2 are shown in Fig. 6. The operating boundary OB2 is lower for 6M GuSCN than for water due to the lower interfacial tension of GuSCN. No boundary OB1 was seen for solutions of SDS and isopropanol because these dramatically lower the interfacial tension, reducing the minimum particle loading to a few micrograms. These systems allow easy particle extraction but are unsuitable for magnet-driven droplet transport.

In biochemical applications, it is often important to deal with viscous biofluids like blood. We therefore investigated the effect of solution viscosity on droplet manipulation, using water droplets with and without 50% glycerin. Fig. 7 shows a sequence of images from which it is clear that when the magnet underneath the droplet is moved, not all the magnetic particles move into the front along the contact line of the drop during transport. This means that not all the magnetic particles loaded into the droplet contribute to the magnetic force. However, this particle loss is much greater in a highly viscous drop (see the 50% glycerin case). As a result, the effective magnetic force acting on the droplet is reduced and the magnet disengagement occurs at a much lower velocity in the case of the droplet with 50% glycerin, than in a pure water droplet. We attribute this to the viscous shear stress inside a moving droplet. Hence more viscous droplets should be manipulated at a lower speed.

3.4 Merging and mixing

In our experiments, we have seen that when the surrounding oil layers are thin, droplet merging always takes place as soon as the two droplets are brought into contact. (see video S1 ESI†). However, for droplets encased in a thick oil shell we had more difficulty promoting droplet coalescence, especially for the small droplets (see video S2 in ESI†). In these cases, a double-core emulsion encompassing both of the discrete water droplets is initially formed when the droplets merge. Because the two aqueous cores are separated by a thick oil medium, the two droplets do not merge spontaneously and in some cases the passive drop is pushed away from the active droplet.

3.5 Design considerations

Based on our experimental and theoretical observations, we here summarize some design and manipulation rules for magnet-driven droplet systems, which typically include a disposable hydrophobic plate, an external Nd–Fe–B magnet and a linear/rotary stage to perform droplet manipulations.

NIH-PA Author Manuscript

NIH-PA Author Manuscript

NIH-PA Author Manuscript

If the magnetic beads are to be used only as a solid support for biomolecular adsorption or bioreaction, then splitting and merging are the most important operations and droplet motion is undesirable. Remember that extracting the superparamagnetic particles from a small droplet less than 5 μL in size on a hydro-phobic surface like spin-coated Teflon®AF is difficult and so should be avoided. Splitting such small droplets can be done on hydrophobic plates (like PTFE plate) that have slightly rough surfaces but to which the particles do not adhere. Confining the droplets within interconnected wells as shown by Shikida *et al*.[23] is also a possible solution but would add to the difficulties of device fabrication. If possible, we recommend ferromagnetic particles for these applications, because their higher magnetic susceptibilities make droplet splitting easier. In addition, the splitting operation depends sensitively on the interfacial tension between the aqueous droplet and the surrounding medium. A thin layer of oil is often indispensable for breakage to occur and surfactants should also be considered if they do not interfere with the desired processes occurring within the droplet.

However, when the magnetic particles are used as a droplet driver and particle extractions are not needed at any time during the procedure, a smooth hydrophobic surface or even a super-hydrophobic surface is desirable. High interfacial tension could in this case facilitate rapid droplet transport. Otherwise, to prevent droplet splitting, a relatively low transport speed should be used, depending on the size of target droplet.

For systems requiring both droplet transport and particle extraction, a smooth hydrophobic surface like the spin-coated Teflon®AF used in this work is preferable. One can then readily switch between droplet movement and particle extraction, using the operating diagram to adjust magnet speed, having precisely controlled the droplet size, oil loading, interfacial tension *etc*., as discussed above. These latter parameters become especially important when the speed of the magnet is confined to a narrow operating range, within which the critical condition for droplet breakup must be accessible.

Conclusions

We have reported an experimental droplet operating diagram containing regions of stable droplet transport, breakup, and magnet release for a droplet manipulation platform consisting of an open hydrophobic plate and a motion-controllable magnet. We demonstrated the conditions under which transport of droplets (from few microliters to hundreds of microliters in volume) can be combined with particle extraction/transfer on such a simple platform. The operating diagram was rationalized by a simple force balance model that includes magnetic, capillary, and frictional forces, and is able to explain semi-quantitatively all experimentally observed phenomena and dependence of the droplet velocity and breakup conditions on droplet parameters, including surface tension, fluid viscosity, and magnetic particle loading. We believe this fundamental study will enhance the understanding, and implementation, of magnetic-bead-containing droplet manipulation systems.

Supplementary Material

Refer to Web version on PubMed Central for supplementary material.

Acknowledgments

This work was supported by the National Institutes of Health (NIAID RO1 AI49541) and by the State of Michigan 21st Century Jobs Fund.

References

1. Whitesides GM. Nature 2006;442:368–373. [PubMed: 16871203]

NIH-PA Author Manuscript

NIH-PA Author Manuscript

NIH-PA Author Manuscript

2. Reyes DR, Iossifidis D, Auroux PA, Manz A. Anal. Chem 2002;74:2623–2636. [PubMed: 12090653]
3. Auroux PA, Iossifidis D, Reyes DR, Manz A. Anal. Chem 2002;74:2637–2652. [PubMed: 12090654]
4. Vilkner T, Janasek D, Manz A. Anal. Chem 2004;76:3373–3385. [PubMed: 15193114]
5. West J, Becker M, Tombrink S, Manz A. Anal. Chem 2008;80:4403–4419. [PubMed: 18498178]
6. Mukhopadhyay R. Anal. Chem 2006;78:1401–1404. [PubMed: 16570390]
7. Teh SY, Lin R, Hung LH, Lee AP. Lab Chip 2008;8:198–220. [PubMed: 18231657]
8. Fair RB. Microfluid. Nanofluid 2007;3:245–281.
9. Srinivasan V, Pamula VK, Fair RB. Lab Chip 2004;4:310–315. [PubMed: 15269796]
10. Schwartz JA, Vykoukal JV, Gascoyne PRC. Lab Chip 2004;4:11–17. [PubMed: 15007434]
11. Lehmann U, Vandevyver C, Parashar VK, Gijs MAM. Angew. Chem., Int. Ed 2006;45:3062–3067.
12. Pipper J, Inoue M, Ng LFP, Neuzil P, Zhang Y, Novak L. Nat. Med 2007;13:1259–1263. [PubMed: 17891145]
13. Pipper J, Zhang Y, Neuzil P, Hsieh TM. Angew. Chem., Int. Ed 2008;47:3900–3904.
14. Garcia AA, Egatz-Gomez A, Lindsay SA, Dominguez-Garcia P, Melle S, Marquez M, Rubio MA, Picraux ST, Yang DQ, Aella P, Hayes MA, Gust D, Loyprasert S, Vazquez-Alvarez T, Wang J. J. Magn. Magn. Mater 2007;311:238–243.
15. Schneider J, Egatz-Gomez A, Melle S, Lindsay S, Dominguez-Garcia P, Rubio MA, Marquez M, Garcia AA. Colloids Surf., A 2008;323:19–27.
16. Ohashi T, Kuyama H, Hanafusa N, Togawa Y. Biomed. Microdevices 2007;9:695–702. [PubMed: 17505884]
17. Nguyen NT, Ng KM, Huang XY. Appl. Phys. Lett 2006;89:052509.
18. Nguyen NT, Beyzavi A, Ng KM, Huang XY. Microfluid. Nanofluid 2007;3:571–579.
19. Sun Y, Nguyen NT, Kwok YC. Anal. Chem 2008;80:6127–6130. [PubMed: 18572956]
20. Sun Y, Kwok YC, Nguyen NT. Lab Chip 2007;7:1012–1017. [PubMed: 17653343]
21. Shikida M, Nagao N, Imai R, Honda H, Okochi M, Ito H, Sato K. J. Micromech. Microeng 2008;18:035034.
22. Shikida M, Takayanagi K, Honda H, Ito H, Sato K. J. Micromech. Microeng 2006;16:1875–1883.
23. Shikida M, Takayanagi K, Inouchi K, Honda H, Sato K. Sens. Actuators, B 2006;113:563–569.
24. Lehmann U, de Courten D, Vandevyver C, Parashar VK, Gijs MAM. Microelectron. Eng 2007;84:1669–1672.
25. Lehmann U, Hadjidj S, Parashar VK, Vandevyver C, Rida A, Gijs MAM. Sens. Actuators, B 2006;117:457–463.
26. Tsuchiya H, Okochi M, Nagao N, Shikida M, Honda H. Sens. Actuators, B 2008;130:583–588.
27. Pamme N. Lab Chip 2006;6:24–38. [PubMed: 16372066]
28. Kim HY, Lee HJ, Kang BH. J. Colloid Interface Sci 2002;247:372–380. [PubMed: 16290477]
29. Hodges SR, Jensen OE, Rallison JM. J. Fluid Mech 2004;512:95–131.
30. Poeckh T, Lopez S, Fuller AO, Solomon MJ, Larson RG. Anal. Biochem 2008;373:253–262. [PubMed: 18022378]

NIH-PA Author Manuscript

NIH-PA Author Manuscript

NIH-PA Author Manuscript

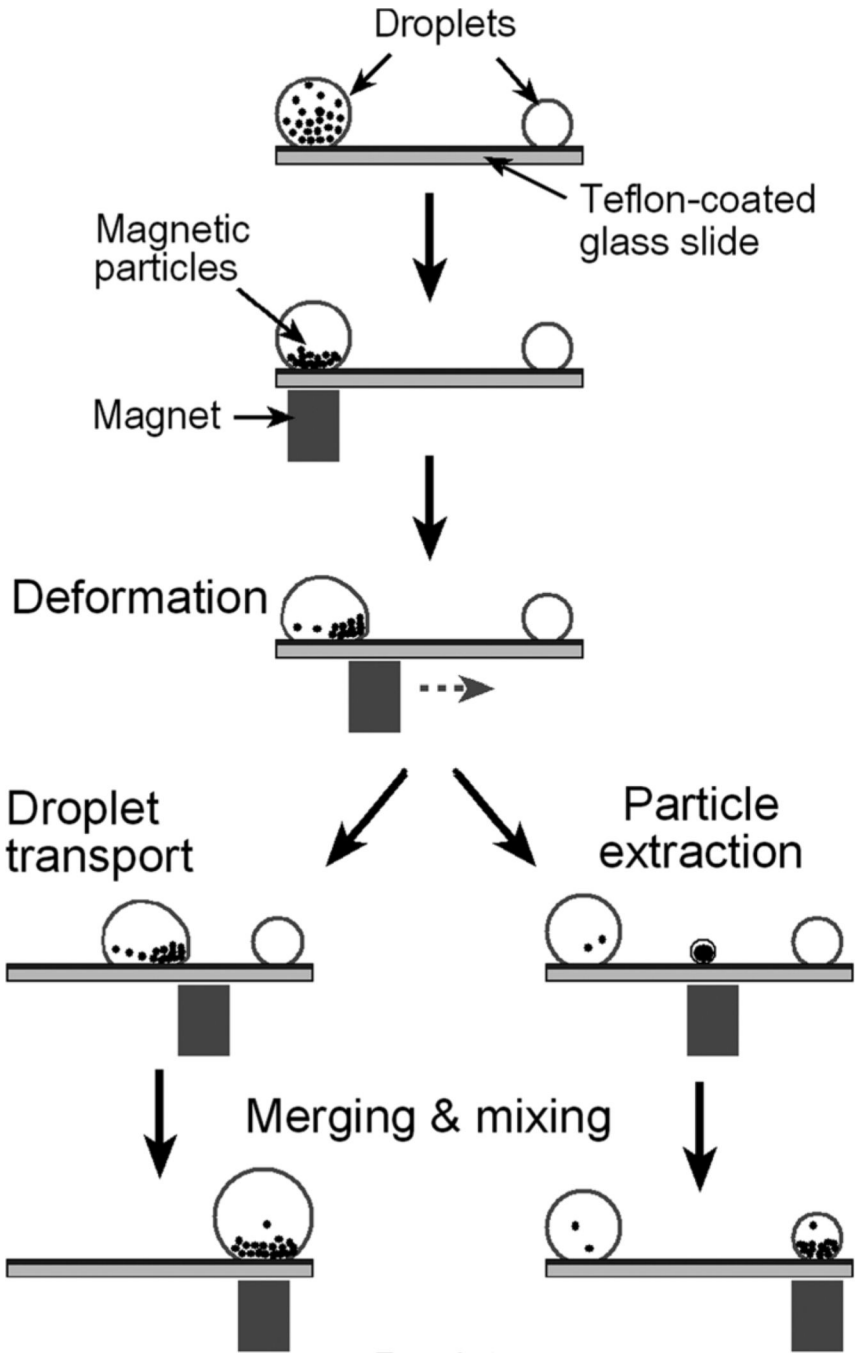

Fig. 1.
Schematic set-up and fundamental operations in a magnet-actuated droplet system.

NIH-PA Author Manuscript
NIH-PA Author Manuscript
NIH-PA Author Manuscript

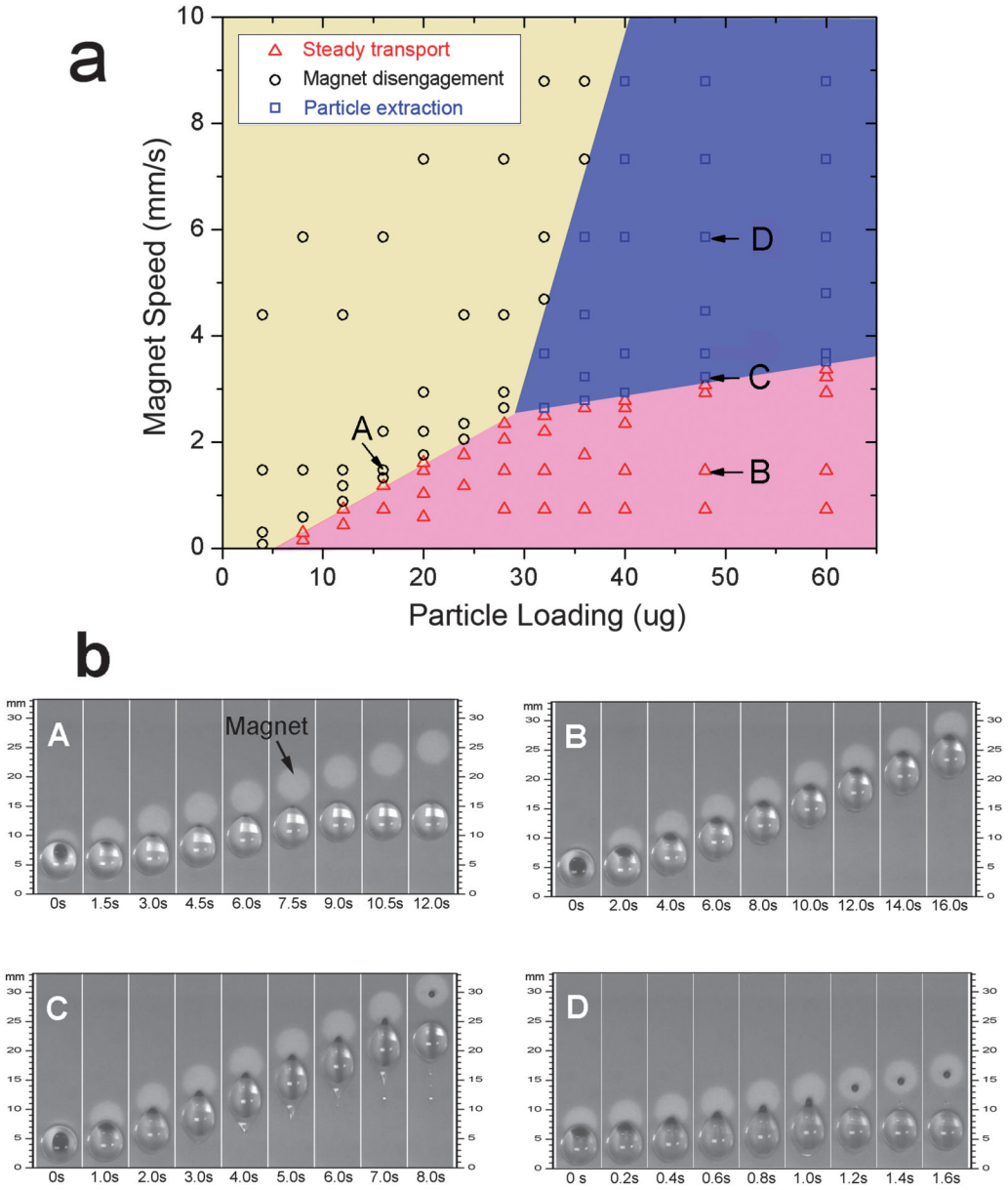

Fig. 2.

(a) Operating diagram showing the outcomes for various magnet velocities and magnetic particle loadings. (b) Video sequences of various operations. A, B, C and D correspond to the four conditions marked on the operating diagram. The testing droplet consisted of a 50 μL water droplet coated by ~0.2 μL of silicone oil. A suspension (~20 μg/μL) of superparamagnetic SiMAG particles (0.5μm diameter) was used for loading.

NIH-PA Author Manuscript

NIH-PA Author Manuscript

NIH-PA Author Manuscript

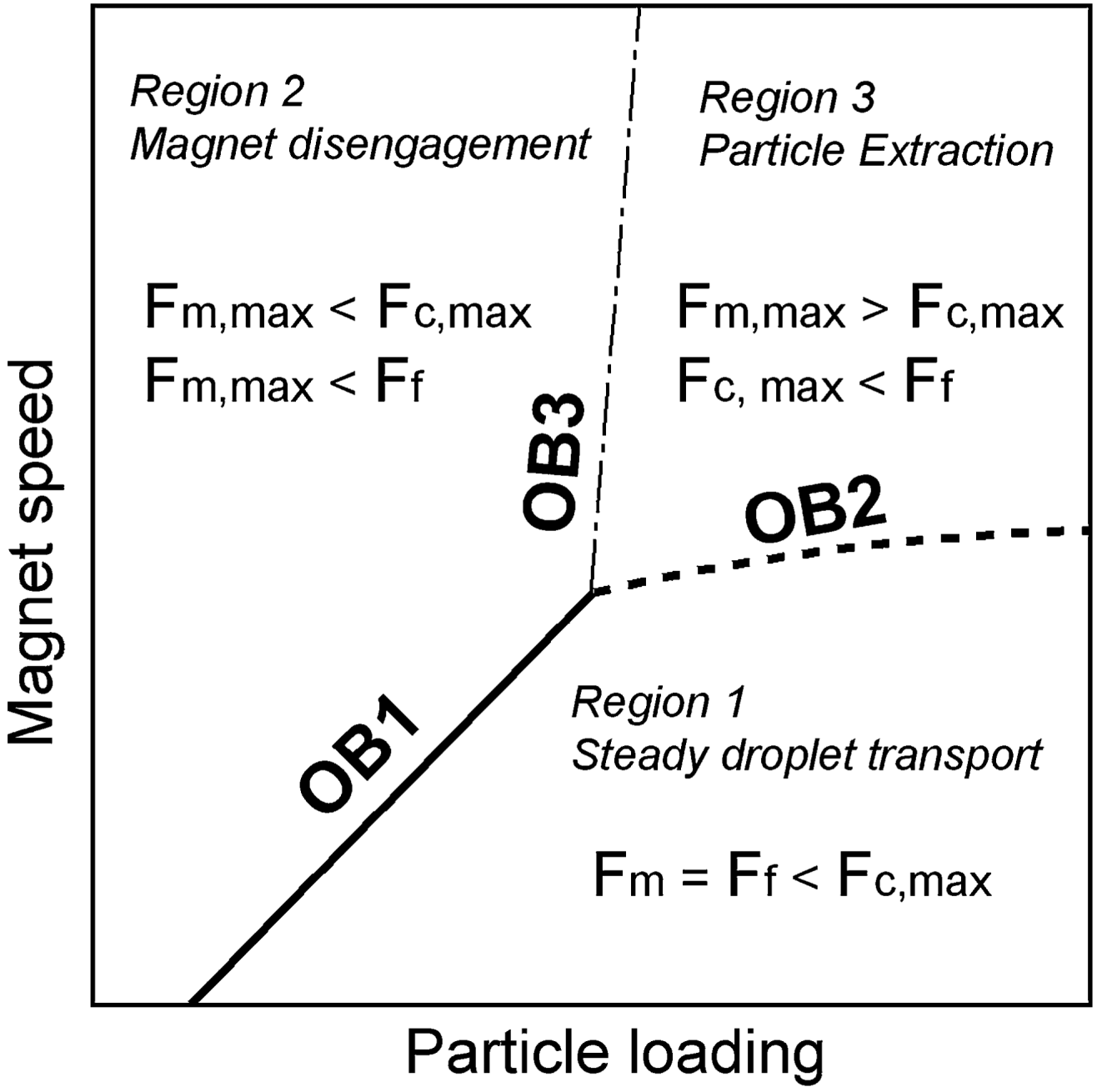

Fig. 3.
Force analysis for the operating diagram. OB1, OB2 and OB3 represent the operating boundaries between the three operation regions.

NIH-PA Author Manuscript
NIH-PA Author Manuscript
NIH-PA Author Manuscript

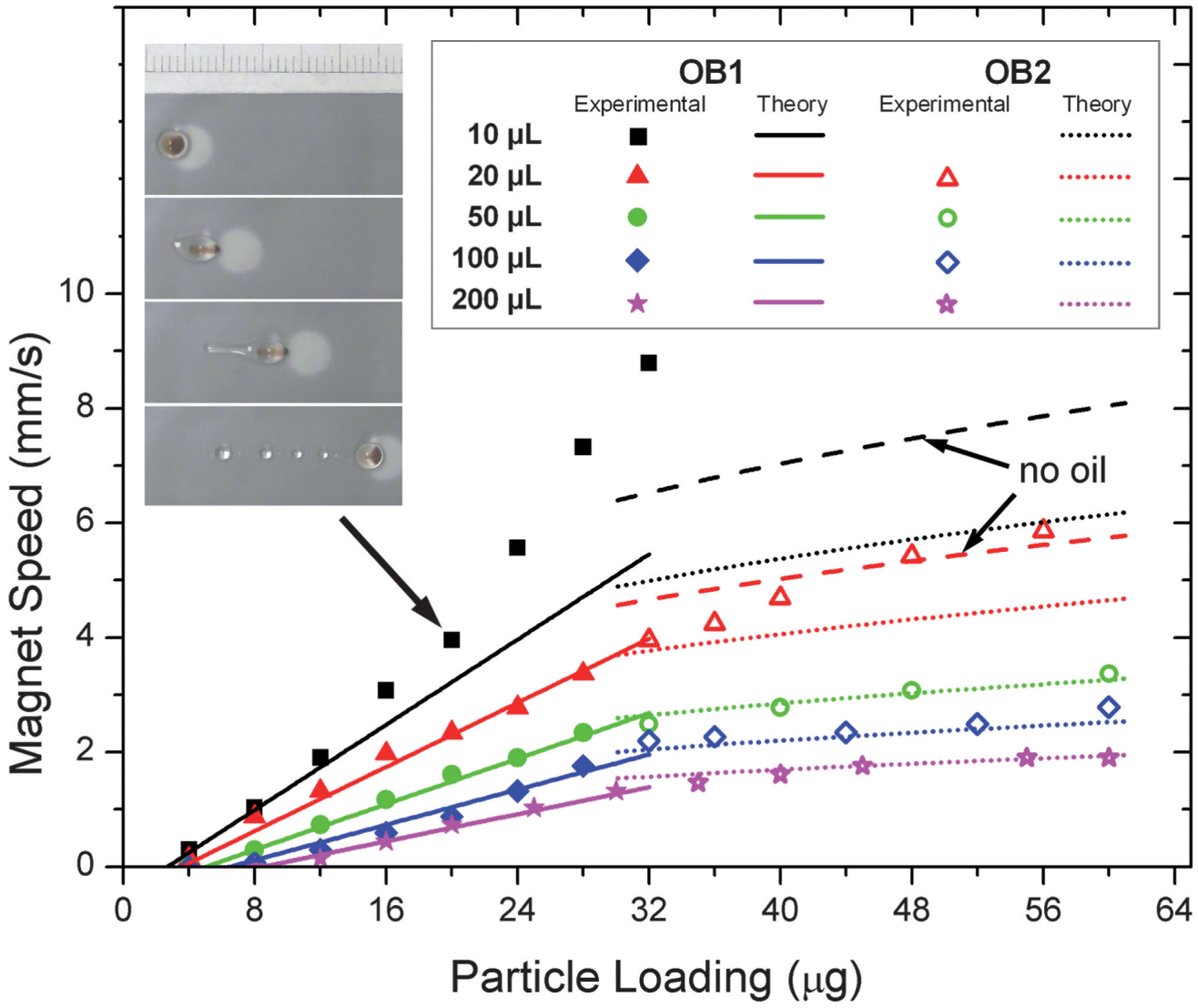

Fig. 4.

Effect of droplet size (10 μl, 20 μl, 50 μl, 100 μl, 200 μl) on the operating diagram. Closed and open symbols represent experimental data for operating boundaries OB1 and OB2, respectively, for the different droplet sizes. The solid lines represent model predictions for OB1. The broken curves refer to predicted OB2 before (dotted) or after (dashed) oil layer fragmentation which has been shown in the inserted video frames. See text for details.

NIH-PA Author Manuscript

NIH-PA Author Manuscript

NIH-PA Author Manuscript

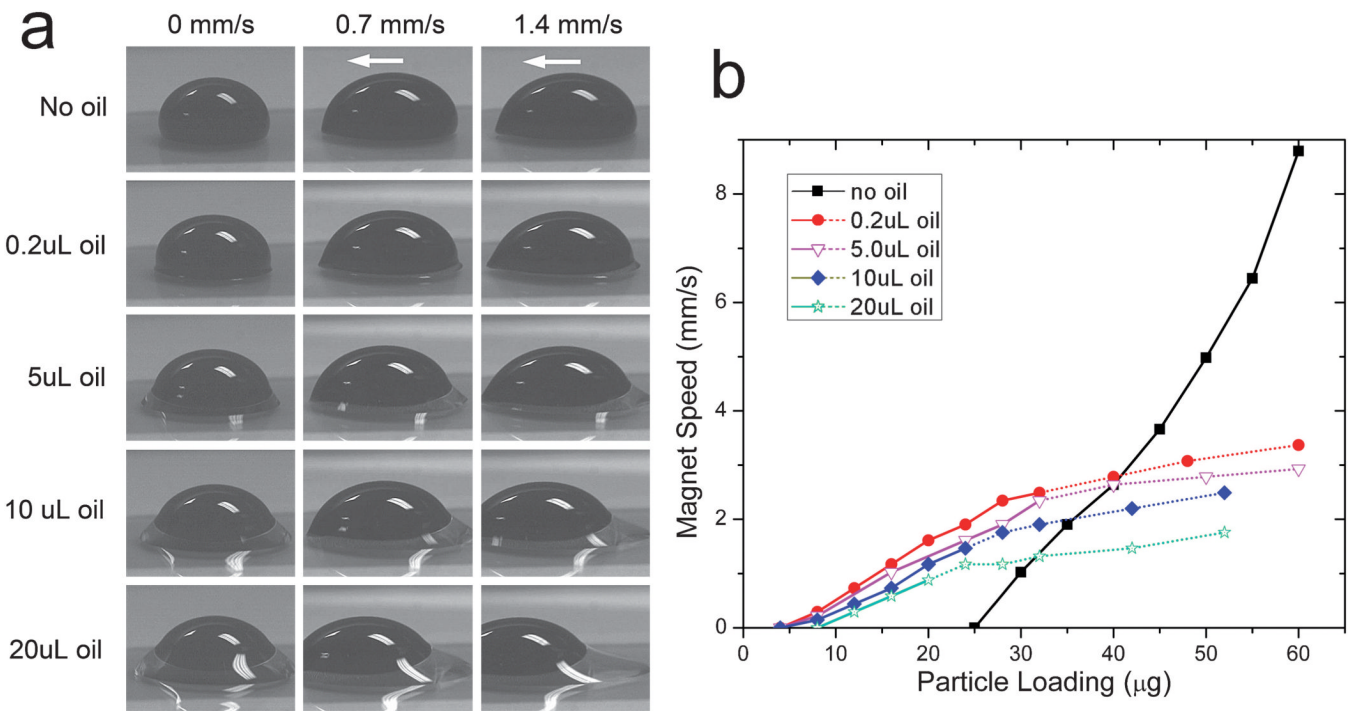

Fig. 5.

Effect of oil loading on dynamic droplet shape (a) and on the operating diagram (b). The white arrows refer to the transport direction. Solid and dotted plots represent operating boundaries OB1 and OB2, respectively. The volume of the aqueous phase was 50 μL in all cases. A stock suspension (~20 μg/μL) of 0.5 μm diameter SiMAG particles was used for the test.

NIH-PA Author Manuscript

NIH-PA Author Manuscript

NIH-PA Author Manuscript

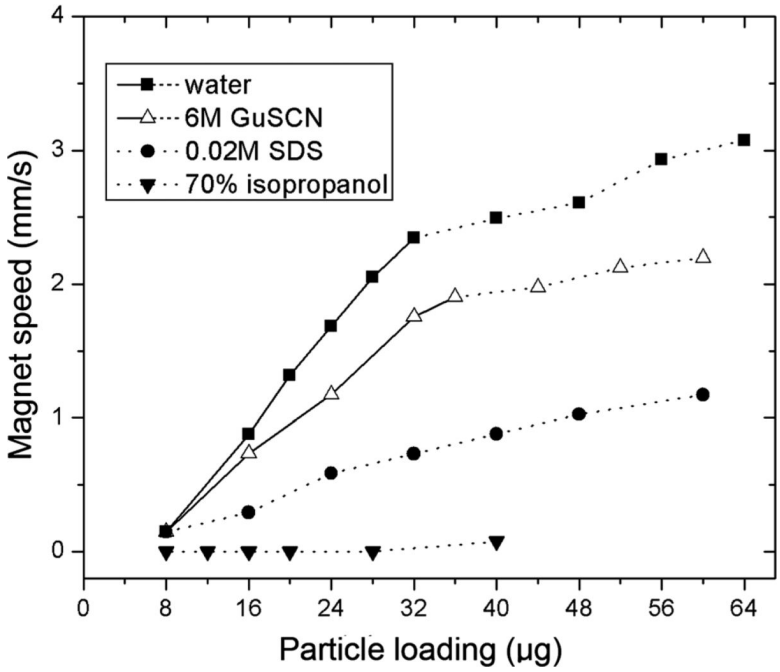

Fig. 6.

Operating boundaries OB1 (solid lines) and OB2 (dashed lines) for droplets of various compositions. All droplets were sealed with 0.2 μL silicone oil and 0.5 μm diameter SiMAG particles were used.

NIH-PA Author Manuscript

NIH-PA Author Manuscript

NIH-PA Author Manuscript

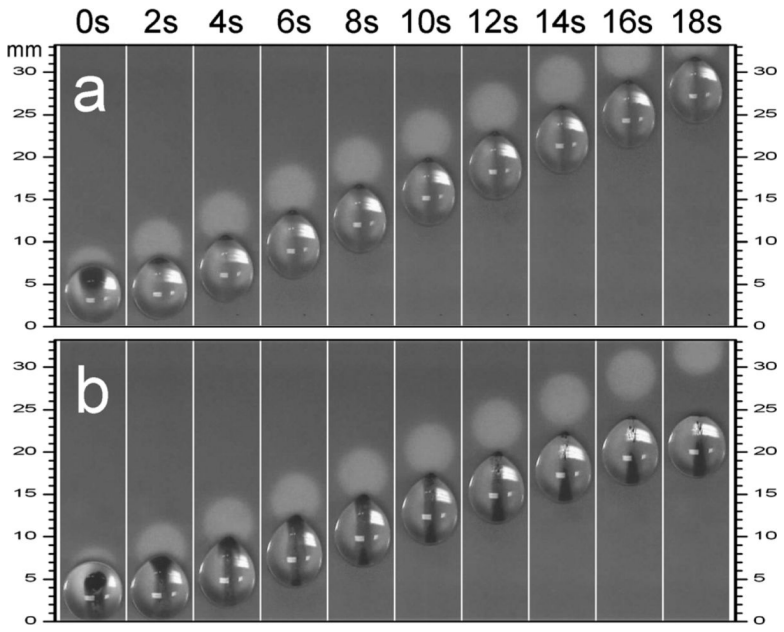

Fig. 7.

Video sequences of moving droplet containing (a) water or (b) 50% (by volume) glycerin in water, showing the effect of solution viscosity on the mobility of encased particles. The droplets were 50μL in volume and sealed with 0.2μL silicone oil. 40μg (*viz.* 0.8 μL suspension) superparamagnetic particles (0.5 μm diameter) were loaded. The velocity of the magnet was 1.5 mm s^{1} in both cases.